Histological and Biochemical Evaluation of the Possible Protective Effect of Thymoquinone Loaded Nanostructured Lipid Carriers Versus Thymoquinone on Cisplatin Induced Testicular Toxicity in Adult Rats

Original Article

Heba G. Ibrahim[1], Moushira Ahmed Zoheir[1], Fatma El zahraa A. Hashem[1], Mariam Zewail[2] and Rehab Ahmed Abdel-Moneim[1]

[1]*Department of Histology and Cell Biology, Faculty of Medicine, Alexandria University, Alexandria, Egypt.*

[2]*Department of Pharmaceutics, Faculty of Pharmacy, Damanhour University, Damanhour, Egypt.*

ABSTRACT

Introduction: Cisplatin (Cis) is considered as a cornerstone in different protocols of chemotherapy. Nevertheless, its utilization is hampered by its toxicity especially on the testis. Thymoquinone (Thq) showed promising antioxidant capabilities against cisplatin induced pathologies. However, owing to its low bioavailability after oral intake, thymoquinone-loaded nanostructured lipid carriers (ThqNLC) have been developed.

Aim of Study: To compare the potential protective effect of ThqNLC versus Thq in mitigating pathological effects of cisplatin on rat testis.

Materials and Methods: Forty-eight adult male albino rats were divided into four groups (n=12) in one month duration experiment: group I, control that was subdivided to three subgroups (Ia, Ib and Ic) that received orally: distilled water, Thq (5 mg/kg daily) and ThqNLC (5 mg/kg daily) respectively, group II received: Cis (3 mg/kg IP injection once daily from day11-day15), group III received: Cis+ Thq, group IV: Cis+ ThqNLC. Testicular affection was assessed via histological studies. Serological markers such as malondialdehyde (MDA), total antioxidant capacity (TAC) and total serum testosterone were evaluated. Additionally, immunofluorescence reaction against PCNA was illustrated by confocal scanning laser microscope.

Results: Cis was associated with disorganization of testicular architecture and depletion of germinal epithelium that was demonstrated by decreased epithelial height and sperms in epididymal lumen. Bizarre- shaped spermatozoa were noticed near tubular lumen. Significant diminution of anti PCNA immune reaction were assessed morphometrically. ThqNLC proved their safety in addition to their role in mitigating testicular toxicity which was superior to Thq alone. This protective potential was obvious through histological and biochemical results that referred to the antioxidant capacity of ThqNLC as highlighted by the marked differences in MDA and TAC levels between the studied groups.

Conclusion: ThqNLC exert more protective effect against Cis-induced testicular toxicity than Thq alone. Therefore, ThqNLC can play an essential role in the field of oncofertility.

Received: 08 September 2022, **Accepted:** 25 September 2022

Key Words: Chemotherapy, cisplatin, infertility, oxidative stress.

Corresponding Author: Heba G. Ibrahim, PhD, Department of Histology and Cell Biology, Faculty of Medicine, Alexandria University, Alexandria, Egypt, **Tel.**: +20 12 2235 5864, **E-mail:** heba.ibrahim@alexmed.edu.eg

ISSN: 1110-0559, Vol. 46, No. 4

INTRODUCTION

Cisplatin- platinum based chemotherapeutic agent- has been viewed as a cornerstone in the treatment of wide range of human cancers such as ovarian, testicular, bladder, lung and liver cancer, in addition to hematological tumors such as leukemia[1]. Despite the efficiency of cisplatin in cancer treatment, its usage is faced by spectrum of serious side effects such as renal, hepatic, cardiac and gonadal toxicity[2]. It was epidemiologically proved that male survivors, especially in cases of testicular carcinoma, leukemias and lymphoma suffered from reduced fertility[3]. This raised the need for new medical field named oncofertility that aims to preserve the gonadal function in patients on cancer therapy[4].

The deleterious effect of cisplatin on DNA is considered as one of the main mechanisms of its action. DNA binding through the N7 position of purine bases, followed by single and double strand breaks then intra- and inter-strand crosslinks result in blockage of DNA transcription, replication and eventually, cell cycle arrest or apoptosis[5,6]. Cisplatin induced testicular toxicity, as reported in previous studies, leads to defective spermatogenesis, together with Leydig cells dysfunction[4,7]. Different strategies were proposed to reach safer cisplatin therapy such as implementation of less toxic new analogues, combination therapy to decrease required doses, or administration of antioxidants either in their original forms or as nanometric formulations[8].

 DOI: 10.21608/ejh.2022.161298.1770

Recently, the herbal medicine has emerged as an essential alternative in treatment of variable medical conditions[4]. In this context, it has been of research interest to investigate the prophylactic role of thymoquinone (Thq) against testicular injury. Thq constitutes the majority of the essential oils present in Nigella sativa seeds (also known as black cumin seed). It exerts its beneficial effects through its powerful antioxidant, immunomodulatory, antiapoptotic and anti-inflammatory properties. It is one of the most widely used protective agents owing to its low toxicity in addition to high efficacy[9]. Its role in ameliorating infertility was explained by multiple mechanisms including improvement of sperm count and motility through enhancement of oxidative phosphorylation enzymes, increase testosterone levels due to maturation of more Leydig cells and potentiating pituitary gonadotropins hormonal action[10].

Interestingly, Thq showed anticancer effect on different cell lines which is attributed to its selective ability to generate reactive oxygen species (ROS) in cancer cells while acting as a protective antioxidant in normal tissues[11]. This dual activity is dose dependent, as lower concentrations promote antioxidant behavior. Thq acquired cytotoxic effect through its conversion to semi quinone catalyzed by copper ions that is known to be elevated in various malignancies[12,13]. Therefore, Thq can potentiate cisplatin therapeutic effect while mitigating its side effects on normal tissues. Despite the beneficial effects of Thq, its oral bioavailability is limited due to its high hydrophobicity, limited absorption and excessive plasma proteins binding[11]. Therefore, implementation of lipid based nanocarriers including solid lipid nanoparticles and nanostructured lipid carriers (NLC) is essential to improve Thq bioavailability. In this regard, they are considered as an excellent alternative for liposomal and polymeric drug delivery systems, particularly for the delivery of lipophilic pharmaceuticals[14].

Nanostructured lipid carriers are considered as the second generation of solid lipid nanoparticles that are composed of a mixture of solid and liquid lipids[15]. Nanostructured lipid carriers are superior to solid lipid nanoparticles as they have higher drug loading ability, stability, decreased burst effect and provide better control of drug release characteristics[16].

In the present study, we aimed to assess the possible protective role of thymoquinone as compared to thymoquinone loaded nanostructured lipid carriers in mitigating cisplatin induced testicular toxicity in rats.

MATERIALS AND METHODS

Animals

Forty-eight adult male albino rats 6-8 weeks old and weighing 150-200 g were obtained from the Animal House of the Physiology Department, Alexandria Faculty of Medicine. The experimental animals were housed in the standard laboratory medium concerning temperature and humidity and 12 h light/dark cycles. The animals were fed standard laboratory diet and tap water ad libitum. Guidelines for care and use of animals, approved by the ethics committee, Faculty of Medicine, University of Alexandria, were followed with IBR No.00012098.

Chemicals

Thymoquinone (product number 274666, purity ≥98) was purchased from Sigma-Aldrich Chemical Co. (St. Louis, USA.). Compritol 888 ATO was kindly provided by Gattefossé (Saint Priest, France). Pluronic F127 was provided by Borg Pharmaceutical Company (Alexandria, Egypt). Oleic acid was purchased from Nice Chemicals (Kerala, India). Cisplatin solution (1mg/ml), Cisplatine®, was purchased from Mylan, S. A. S., Saint-Priest, France.

Methods

Preparation of ThqNLC

ThqNLC were prepared by the melt emulsification method previously reported by Zewail et al[17]. Briefly, Compritol was melted at a temperature higher than its melting point by 10 ºC, then oleic acid and different amounts of Thq (from 10-60 mg) were added to the molten lipid. The ratio between compritol and oleic acid was (70: 30 %w/w). An aqueous phase composed of 0.4% pluronic 127 was heated to the same temperature, added to the lipid phase and ultrasonicated at 60 mA for 4 min. The formed pre-emulsion was added to an external aqueous phase composed of deionized water, and then the produced emulsion was ultrasoniacted for 4 min in an ice bath to obtain the final nano-dispersion.

Characterization of ThqNLC

Measurement of particle size and zeta potential

Formulations were subjected to particle size, polydispersity index (PDI) and ζ potential analysis by using Malvern zeta sizer Nano ZS, Malvern Instruments, (Malvern, UK). Formulations were diluted with deionized water. Samples for particle size measurements were placed in square glass cuvettes, while those for ζ potential were placed in clear disposable zeta cells. Measurements were repeated in triplicates[18].

Fourier transform infrared spectroscopy (FTIR)

FTIR spectra for different components incorporated in ThqNLC were recorded by (Agilent Cary 630 FTIR spectrometer, USA) at 500 – 4400 cm^{-1}[19].

Morphological examination

The morphology of the selected ThqNLC was investigated after staining with uranyl acetate by transmission electron microscope (TEM); (JEOL-JSM 1400 Plus, Tokyo, Japan)[20].

Measurement of entrapment efficiency and percentage drug loading

The amount of unencapsulated drugs was measured by

the ultrafiltration method via Centrisart®-I tubes. Briefly, ThqNLC were centrifuged for 30 min at 5000 rpm, then the amount of unencapsulated drug in the supernatant was determined directly through spectrophotometric analysis at 258 nm using the following equation[21].

$$\% \text{ EE (indirect)} = \frac{\text{(Total drug concentration-concentration of unencapsulated drug)}}{\text{(Total drug concentration)}}$$

Percentage drug loading (DL) was determined by measuring drug concentration in a given weight of freeze-dried nanocarriers.

$$\% \text{ DL} = \frac{\text{(Concentration of encapsulated drug)}}{\text{(Weight of nanocarriers)}} \times 100$$

Drug release study

In vitro release studies were performed in a dialysis bag (Visking® 36/32, 28mm, MWCO 12000-14000, Serva, USA) for selected Thq formulation and Thq suspension. Dialysis bags containing ThqNLC and Thq suspension were immersed in 75 ml phosphate buffer saline (PBS), pH 7.4 to ensure sink conditions and incubated in a shaking water bath at 37ºC ± 0.2 ºC and 100 rpm. At different time intervals, samples were withdrawn and replaced with fresh PBS. Thq concentration was determined spectrophotometrically at 258 nm[20,22].

Stability of ThqNLC

Storage stability study was conducted by storing ThqNLC at 4 °C. Any changes in particle size and entrapment efficiency were verified after 3 months[23].

Experimental design

The animals were randomly allocated in four groups 12 rats each after one week of adaptation.

Group I: Control group, (12 rats) was subdivided into 3 subgroups: Ia (distilled water), received distilled water -which is the vehicle of thymoquinone- orally for 30 days, Ib (Thq) received thymoquinone in a daily dose of 5 mg/kg body weight orally by gastric gavage for 30 days, Ic (ThqNLC) received thymoquinone loaded on nanostructured lipid carriers in an equivalent dose by gastric gavage for 30 days[24].

Group II: Cisplatin Group (Cis gp): received distilled water orally for 30 days. From day 11 of the experiment, intraperitoneal injection of cisplatin was given at a dose of 3 mg/kg body weight for five consecutive days[25].

Group III: Cisplatin + Thymoquinone (Cis+ Thq gp): received thymoquinone in a daily dose of 5 mg/kg body weight orally by gastric gavage for 30 days and cisplatin at a dose of 3 mg/kg body weight for five consecutive days starting from day 11 of the experiment[24,25].

Group IV: Cisplatin + Thymoquinone loaded on nanostructured lipid carriers (Cis +ThqNLC gp): received thymoquinone loaded on nanostructured lipid carriers in a daily dose of 5 mg/kg body weight orally by gastric gavage for 30 days and cisplatin at a dose of 3 mg/kg body weight for five consecutive days starting from day 11 of the experiment[24,25].

Sampling

On day 31, 24 hours after receiving the last dose, blood samples were collected from retro-orbital venous plexus then centrifuged for 10 min to obtain serum for biochemical analysis. Both testes are obtained for histological study after rats euthanasia[26].

Serum biochemical study

Oxidative marker assay

Serum Malondialdehyde (MDA) levels were measured as markers of oxidative stress via colorimetric assay using kits of the Biodiagnostic company (Giza, Egypt). MDA level was determined as Thiobarbituric Acid Reactive Substances (TBARS). Lipid peroxidation yielded peroxides that combined with thiobarbituric acid by heating resulting in a colored compound that was measured at 534 nm by a Humalyzer junior photometer (Human Diagnostics, Germany)[27].

Total Antioxidant Capacity (TAC)

The antioxidative capacity was assessed according to Koracevic et al.[28] through the reaction of serum antioxidants with a certain amount of exogenously added hydrogen peroxide (H_2O_2). The remaining H_2O_2 was measured colorimetrically by an enzymatic reaction which included the conversion of 3,5, dichloro 2–hydroxybenzenesulfonic to a colored agent measured at 500 – 510 nm by a Humalyzer junior photometer (Human Diagnostics, Germany). The kit was purchased from Biodiagnostic company (Giza, Egypt).

Total Testosterone estimation:

Serum total testosterone levels were measured using Enzyme Linked Immunosorbent Assay (ELISA) kit (BioCheck Incorporation, USA) by following the kit protocol[29].

Histological study

Light microscopy

The right testis and cauda epididymis were dissected. Specimens from the testis were divided into two groups. The first group was fixed in Bouin's solution to maintain cytoarchitecture of the testicular tissue. Cauda epididymis specimens were fixed in phosphate buffered formol saline. These specimens were further processed for staining by hematoxylin & eosin (H&E) stain[30,31]. Olympus bright field light microscope (equipped with a digital camera) was used to get light microscopic images at the Center of Excellence for Research in Regenerative Medicine and its Applications (CERRMA), Faculty of Medicine, University of Alexandria. The other group of testicular specimens were fixed in phosphate buffered formol saline

for immunofluorescence assessment.

Immuno-fluorescence study

Deparaffinized sections of the testis were gradually rehydrated by using descending ethanol grades then washed in deionized water. According to the antibody kit, the buffer was added to the sections then after10 min the mouse anti-proliferating cell nuclear antigen (PCNA) primary antibodies were added. Specimens were kept overnight in a temperature about 4°C. Then the slides were incubated at 37°C with goat anti-mouse secondary antibodies conjugated with Alex Fluor 555 (Invitrogen, Cat # A-21422; excitation/emission wave lengths 555/580 nm). After washing, DNA counterstaining with DAPI (4′,6-diamidino-2-phenylindole) (Sigma-Aldrich, Czech Republic) was done.

The stained sections were examined using confocal laser scanning microscopy (Leica TSC SPE II/DMi 8) at CERRMA, Faculty of Medicine, Alexandria University. The photomicrographs were morphometrically analyzed for intensity of fluorescence using an image analysis software NIH Fiji© program[32,33].

Transmission electron microscopy (TEM)

For ultra-structural study, the left testes were cut to 1 mm^3 cubes and fixed in 2.5% phosphate buffered glutaraldehyde at 4 °C[34]. Electron micrographs were obtained by TEM (JEOL-JSM 1400 Plus, Tokyo, Japan) in the Electron Microscopy Unit, Faculty of Science, University of Alexandria.

Morphometric study and statistical analysis

Relative assessment of the sperm count was performed by estimating the fraction occupied by spermatozoa as a percentage from the total epididymal lumen surface area. Ten random H&E stained images from each group, total 40 images were examined[35].

Twenty rounded or near oval seminiferous tubules (ST) were randomly chosen from sections at (×100 magnifications) of each group to measure the height of germinal epithelium. First, tubular diameter (T) was obtained as the average length of two perpendicular axes measured in each ST. Second, the luminal diameter (L) was obtained as an average of two perpendicular readings of the same tubules L= (L1+L2)/2. Finally, epithelial height (E) was obtained by using this formulation E= T- L.

The surface areas and diameters of different groups were blindly measured using NIH Fiji© program and the results were compared statistically[36]. All numerical data were expressed as median (min-max). Differences were considered statistically significant at $p < 0.05$ calculated by Kruskal-Wallis test and Mann-Whitney test for pairwise comparison[37].

RESULTS

Characterization of ThqNLC

Colloidal characteristics of ThqNLC

The prepared nano-dispersion was slightly yellowish in color. (Table 1) showed the colloidal characteristics of the prepared formulations.

Particle size, PDI, zeta-potential

Plain NLC (F1) showed average particle size of 198.2 ± 0.793 nm and carried negative surface charge of - 13.7 mV (Figure 1). and this may be attributed to the role of oleic acid in inducing negatively charged uncoated NLC. ThqNLC had higher zeta potential values compared to F1. By increasing Thq concentration, NLC surface charge increased. Zeta potential of F2 (containing 10 mg Thq) and F6 (containing 60 mg of Thq) were -23.4 and -16.4 mV, respectively.

Nano-formulation's particle size is a crucial factor that affects its cellular uptake and eventually influences their biopharmaceutical performance. Particle size of Thq loaded formulations ranged from 177.5 (F5) to 196.2 nm (F6) as illustrated in (Table 1) Also, the PDI values reflect the degree of system homogeneity. The present results confirmed the formation of homogenous blank and ThqNLC preparations with PDI values of (0.241 and 0.235, respectively).

FTIR spectroscopic analysis

Thq displayed several characteristic peaks (Figure 2A). C=O stretching was observed at 1657 cm^{-1}. At 2918 and 1360 cm^{-1} peaks corresponding to CH stretching and CH bending were observed.

Compritol characteristic peaks were observed at 1738 and 2849 cm^{-1} (Figure 2B), which correspond to (C–O stretching) and (C–H stretching), respectively. Methylene groups displayed several frequencies in the area between 721 and 1468 cm^{-1}.

In NLC spectrum (Figure 2C), only peak shifts were observed with new additional peaks indicating absence of chemical interactions between NLC components. C=O peak was shifted to 1735 cm^{-1} and C-H bending was shifted to 1392 cm^{-1}.

Morphological characterization

TEM micrograph of selected ThqNLC formulation (F5) revealed that it was spherical in shape and its size ranged from 68.66 nm to 91.64 nm that lies within the nano size. No drug crystals were noted indicating efficient Thq encapsulation within the prepared NLC. (Figure 2D)

Entrapment efficiency (EE) and percentage drug loading (% DL)

Lipid nanocarriers including NLC are considered the

formulations of choice for encapsulation of lipophilic drugs[37]. Percentage EE of the prepared NLC ranged from 84.67 % (F2) to 97.92 % (F6). Percentage DL ranged from 5.92 % to 27.56 % (Table 1).

F5 was selected for further characterization as it had suitable particle size (177.5 nm), PDI (0.235) less than 0.5 that ensured the homogeneity of the dispersion. Also, F5 had a high entrapment efficiency percentage of about 96.9 %. F6 was excluded as drug expulsion was noted during storage.

In vitro drug release and release kinetics

The in vitro release profile of Thq suspension and F5 was illustrated in Fig. 2E. F5 showed a biphasic release pattern with about 25 % burst effect (Figure 2E Inset) followed by sustained Thq release for 48h.

Stability

Storage of ThqNLC for 3 months at 25 ºC resulted in increasing their particle size from 177 ± 1.36 to 189.7 ± 2.83 nm. Zeta potential slightly increased to - 18.7 while there was no change in % EE after the storage period. (Figures 1E, 1F)

Serological markers Results

Serum malondialdehyde (MDA) levels

Serum MDA levels showed a statistically significant increase in group II (Cis) compared to control group (p=0.019). The median level of MDA in groups III (Cis+ Thq) and IV (Cis+ThqNLC) was 8.4(5.3- 10.56), 7.22(6.4-9.0) nmol/ml respectively which was significantly less than that of group II (Cis). There was no statistically significant difference neither between groups III and IV nor the control group *P*> 0.05. (Figure 3A)

Serum total antioxidant capacity (TAC) levels

Cisplatin administration caused a statistically significant decrease in the median level of serum TAC in group II 0.64(0.5-0.8) mμ/L compared to the control group 1.25(1-1.54) mμ/L. Although Thq intake in group III increased the TAC, its median level 1(.76-1.17) mμ/L was not significantly exceeding that of group II. However, ThqNLC succeeded to elevate median level of TAC level in group IV (Cis+ThqNLC) 1.14 (0.95-1.3) mμ/L significantly above that of group II to be in the same range as the control groups. (Figure 3B)

Total serum testosterone

The median level of total serum testosterone in group II (Cis) 0.03(0.03- 0.36) ng/ml was significantly decreased as compared to group I 0.955(0.36- 1.09) ng/ml. Meanwhile, testosterone level was increased in groups III and IV to be 0.78 (0.33-1.8) and 0.86 (0.45-1.4) ng/ml respectively, expressing significant rise in comparison to group II. (Figure 3C) No statistically significant difference between groups III, IV was illustrated.

Histological results

Light microscopic results

Light microscopic examination of sections of the testis in the control **group (I)** revealed the normal testicular tissue morphology. The sections showed a regular outline of ST with evident spermatozoa in their lumina. ST appeared lined by the germinal epithelium composed of spermatogenic cells and Sertoli cells in between. Groups of Leydig cells were seen scattered between STs (Figure 4).

Group II: Cisplatin administration in group II rats was associated with disorganized testicular architecture. The ST depicted irregular outline and wide interstitial spaces along with eosinophilic hyaline material in the lumina of ST and in the interstitial spaces. The lining epithelium appeared detached from the basement membrane in most of the ST. Germinal cell depletion ranged from being focal in some ST to almost complete loss in others with subsequent lumen dilation and decreased epithelial height were observed. Marked cytoplasmic vacuolation and dark pyknotic nuclei were noticed in some spermatogenic cells. The lumina showed sloughed pyknotic cells and remnants of spermatozoa. (Figure 5)

Group III: Thq intake along with cisplatin, in group III rats, partial improvement in the general architecture of the testicular tissue was noticed. The germinal epithelium showed apparently increased height. Forming spermatozoa were seen in the lumen of some ST, while others revealed detached spermatogenic cells. (Figure 6A). Spermatogonia in some ST depicted vacuolated cytoplasm and darkly stained nuclei. (Figure 6B)

Group IV: ThqNLC administration in group IV resulted in restoration of the general architecture of rat testis. Most of the ST appeared nearly normal with regular outlines and were lined by well-arranged layers of the germinal epithelium with spermatozoa filling the lumen. Few ST depicted wider lumina with a relative decrease in spermatozoa. (Figures 6C,6D).

Morphometric analysis

The percentage of epididymal lumen surface area occupied by spermatozoa

Measuring the fraction of the total luminal area occupied by spermatozoa revealed that cisplatin in groups II and III caused statistically significant deterioration in the percentage of surface area occupied by sperms 17.96 (14.26-24.1) % and 48.13 (36.12-51.6) % respectively, in comparison to control group (group I) (p<0.0001*). No marked statistical difference was noticed between groups II and III. (Figures 7A-7D)

Utilization of ThqNLC in group IV restored the spermatozoa surface area 74(56.8-78.35) statistically

significant improvement in group IV compared to the effect of Thq in group III (p<0.0001*). (Figure 7E)

Height of the seminiferous epithelium

In group II, a significant decrease in the median of epithelial height was noticed in comparison to control group I (p<0.0001*). The seminiferous epithelial height in group III was significantly decreased as compared to control group but showed no statistically significant difference as compared to group II. Group IV showed a significant increase in the height of seminiferous epithelium compared to groups II and III (p<0.0001*) but showed no significant difference as compared to control. (Figure 9A)

Immunofluorescence microscopic results

The control group revealed immunofluorescence activity illustrating immune reaction against PCNA in the basally located cells in seminiferous tubules. (Figure 8) The reaction was allocated in the nuclei as confirmed by DAPI nuclear staining. Diminished immunofluorescence was reported in group II that was statistically significant in comparison to the control group. (Figure 8B) In group III, the immunofluorescence was partially restored at intensity and was significantly less than that of control group. However, in group IV the fluorescence intensity of PCNA was increased to be significantly higher than groups II, III (p<0.0001*). (Figures 8,9B)

Electron microscopic results

Control group revealed normal ultrastructure of the seminiferous epithelium. Seminiferous tubules appeared lined by subsequent rows of different stages of spermatogenic cells with Sertoli cells in between. (Figure 10)

Group II revealed marked affection of Sertoli cells and the spermatogenic cells lining the seminiferous tubules. Wide spacing between Sertoli cells and spermatogenic cells and interruption of Sertoli- Sertoli junctional complex were illustrated. The cytoplasm of Sertoli cells depicted vacuolations and their mitochondria showed swelling, vacuolations and some appeared with abnormal shapes; as annular-shaped mitochondrion that forms a circle around cytoplasmic components that appeared to be adjacent to the nucleus and lysosomes (Figures 11A, 11B). Primary spermatocytes showed dilated perinuclear cisternae, distorted mitochondria, and excessive cytoplasmic vacuolations. Spermatids exhibited multiple nuclear abnormalities; chromatin dissolution, shrinkage, outline irregularity, and nuclear envelope interruption. (Figures 11C,11D) Spermatozoa exhibited bizarre shape, the head region revealed abnormal morphology of the acrosomal cap, while tail cross sections showed excessive vacuolated residual cytoplasm and swollen mitochondria with distorted cristae. (Figures 11E, 11F)

Group III revealed mild improvement in the ultrastructural features of seminiferous tubules. Sertoli cells showed interrupted junctional complex, cytoplasmic vacuolation, swollen mitochondria with partial loss of cristae. (Figures 12A, 12B) Primary spermatocytes showed mild cytoplasmic vacuolation and occasionally distorted swollen mitochondria. Spermatids depicted cytoplasmic rarefaction, deformed mitochondria with disrupted cristae. (Figure 12C) The developing spermatozoa depicted abnormalities in the acrosomal cap and excessive cytoplasm in subacrosomal space. The middle pieces of the tail region appeared nearly normal. (Figures 12D, 12E)

In group IV, Sertoli cells appeared nearly normal with its indented nucleus, tripartite nucleolus, and well-developed junctional complex with minimal interruption. Spermatogonia rested on basal lamina with normal looking cytoplasm, however, the nucleus showed dilated perinuclear cisterna. (Figure 13A) Primary spermatocyte appeared nearly normal with nucleus showing evident synaptonemal complexes, some elongated mitochondria with well-developed cristae were noticed. (Figure 13B) Spermatids appeared nearly normal with well-organized peripheral mitochondria, yet some nuclei showed mild degree of chromatin dissolution. (Figure 13C) The developing spermatozoa showed normal -like pattern, while few middle piece segments depicted excess residual cytoplasm. (Figures 13D,13E)

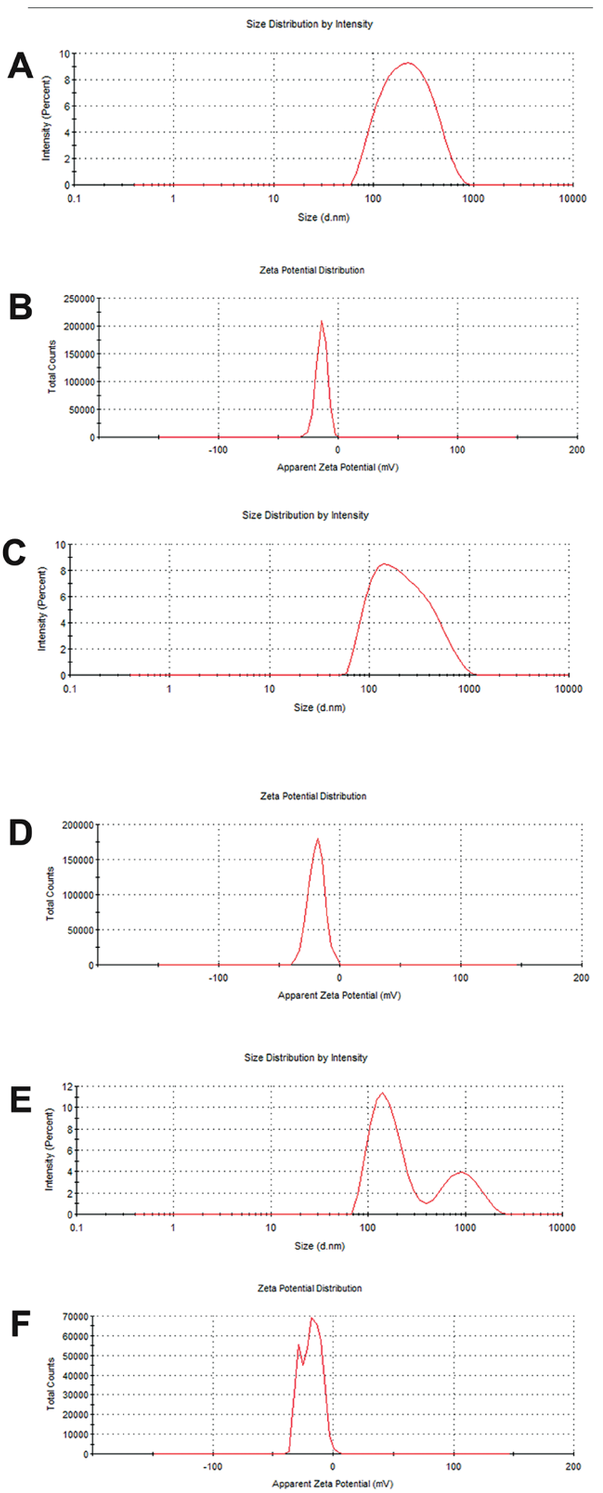

Fig. 1: A; Hydrodynamic size distribution of blank NLC by intensity. B; Zeta potential of blank NLC by intensity. C; Hydrodynamic size distribution of ThqNLC (40 mg Thq) by intensity. D; Zeta potential distribution of ThqNLC (40 mg Thq). E; Hydrodynamic size distribution of ThqNLC (40 mg Thq) after 3-month duration by intensity. F; Zeta potential distribution of ThqNLC (40 mg Thq) after 3-month duration.

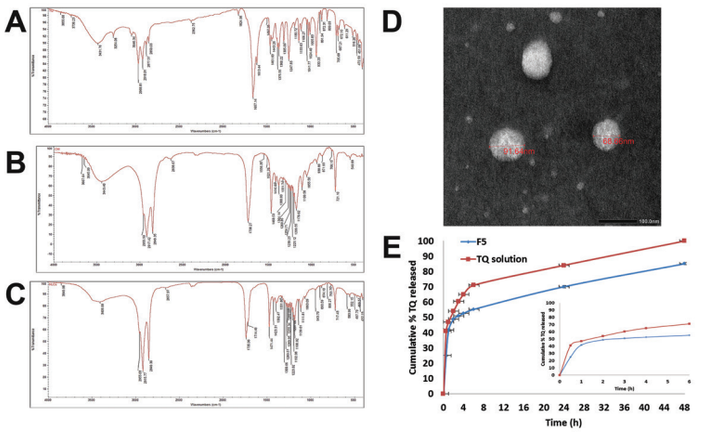

Fig. 2: A; FTIR spectrum of Thq. B; FTIR spectrum of Compritol. C; FTIR spectrum of ThqNLC. D; TEM micrograph of ThqNLC. (Mic.Mag.X60 000). E; Cumulative percentage of Thq released during 48h. Inset illustrates Cumulative % of Thq released within the first 6h.

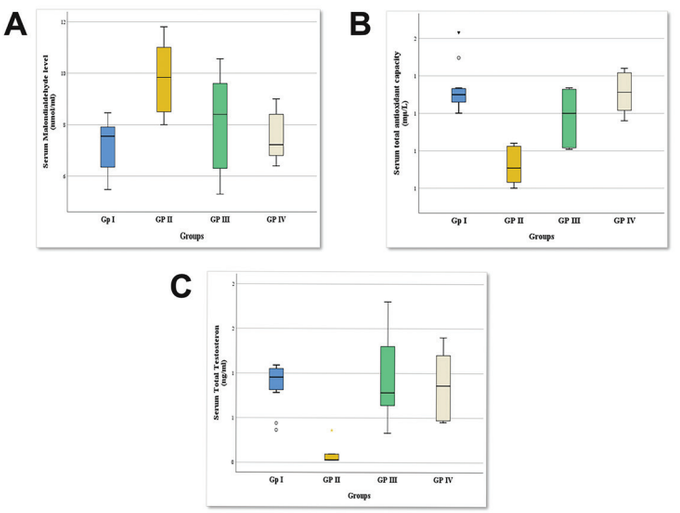

Fig. 3: A; Comparison between the study groups according to Serum Malondialdehyde level. Significance detected between Group I vs Group II. B; Comparison between the study groups according to serum total antioxidant capacity. Significance was detected between Group II vs {Group I & Group IV}. C; Comparison between the study groups according to serum total testosterone. Significance detected between Group II vs {Group I & Group III &Group IV}. Values represent median (min-max) (n = 12). Statistical differences according to Kruskal-Wallis test and Mann-Whitney test for pair wise comparison at (p< 0.05).

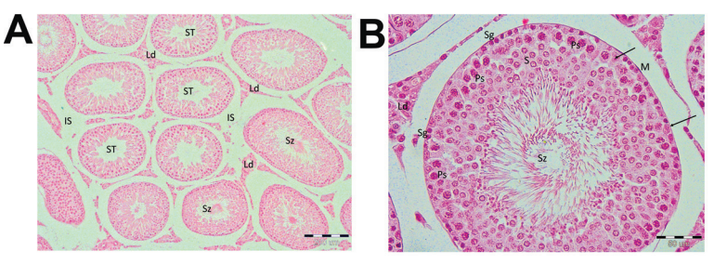

Fig. 4: H & E stained sections of the control group

A, B; Regular cross sections in seminiferous tubules (ST) appear lined by Sertoli cells with their large pale nuclei (arrow), spermatogonia resting on basement membrane (Sg), primary spermatocytes (Ps) with large, rounded nuclei and condensed chromatin. Early spermatids are seen with regular rounded nuclei (S). Spermatozoa (Sz) are seen filling the lumen. The interstitial spaces (IS) show groups of Leydig cells (Ld) with eosinophilic cytoplasm. M: myoid cells. Microscopic magnification A x 100, B x 400. Scale bar: (A) 200µm, (B) 50µm.

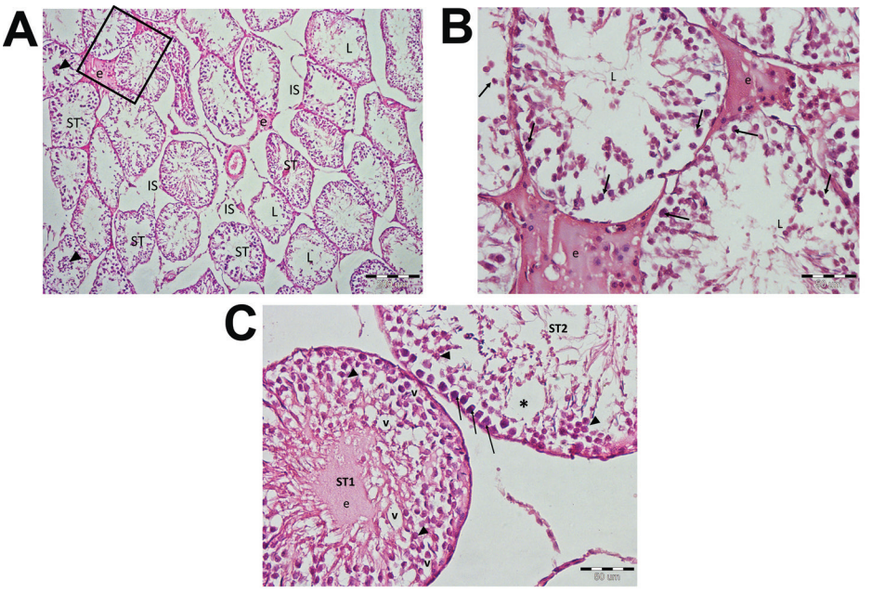

Fig. 5: H & E stained sections of Cis group, A; Distorted seminiferous tubules (ST) with irregular outline and wide interstitial spaces (IS) are seen. Sloughed spermatogenic cells (arrowheads) are seen in the lumina of some ST. Depletion of spermatogenic cells and decreased epithelial height with subsequent lumen dilation (L) are noticed. B; At higher magnification, some sloughed spermatogenic cells are seen in the lumina (L). Basally located spermatogenic cells with dark pyknotic nuclei (arrows) are seen detached from basal lamina. Eosinophilic hyaline exudate (e) is noticed between ST. C; Dark pyknotic spermatogenic cells (arrowhead) with excessive vacuolation (V) are seen. ST1 shows intraluminal hyaline eosinophilic material (e) while ST2 depicts areas of focal loss of germinal epithelium (*). Note dark shrunken spermatogonia (arrows) resting on the basal lamina with dense nuclei, wide intercellular spaces and remnants of spermatids in the lumen. Microscopic magnification (A) x 100, (B & C) x 400. Scale bar: (A) 200µm, (B& C) 50µm.

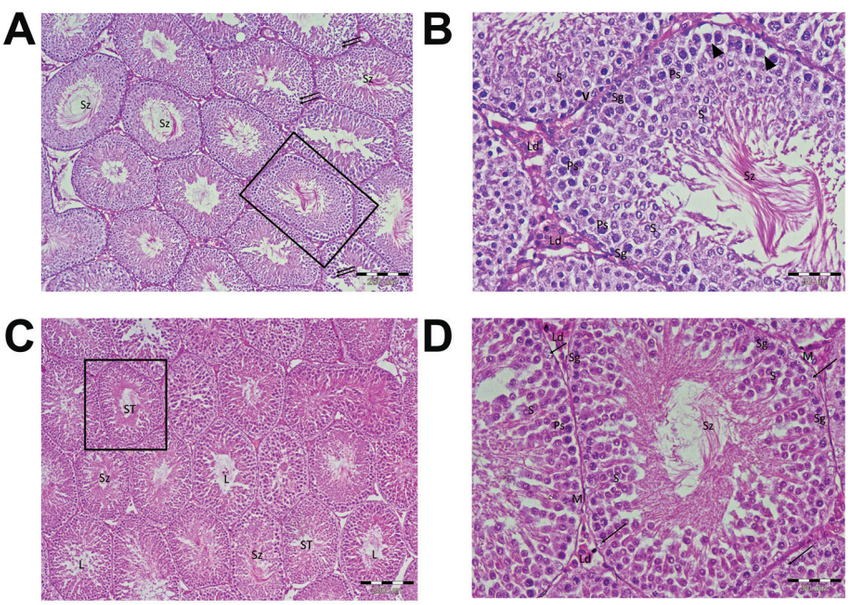

Fig. 6: H & E stained sections of groups III & IV, A, B; Group III, the effects of Thq on Cis treated rat testis. A; Seminiferous tubules depict regular outlines, most of them appear lined by stratified germinal epithelium with forming spermatozoa (Sz) in the lumen, while some others depict detached spermatogenic cells (double arrow). B; At a higher magnification, spermatogonia are noticed lying on basal lamina (Sg). Primary spermatocytes (Ps) are seen with their large nuclei. Some are separated by wide intercellular spaces (arrowhead) while others show vacuolated cytoplasm (V). S: early spermatid. C, D; Group IV, the effects of ThqNLC on Cis treated rat testis. C; Regular cross sections in seminiferous tubules (ST) are lined by germinal epithelium and growing spermatozoa (Sz) project into the lumen. Few ST show apparently wider lumen (L) and decrease in spermatozoa. D; At a higher magnification, spermatogonia (Sg) are seen resting on basement membrane. Sertoli cells depict large pale nuclei (arrow). Primary spermatocytes (Ps) show large nuclei with condensed chromatin pattern. Early spermatids are seen with regular rounded nuclei (S). Sz: spermatozoa fill the lumen of ST. Ld: The interstitial cells of Leydig. M: myoid cells. Microscopic magnification (A & C) x 100, (B&D) x 400. Scale bar: (A, C) 200µm, (B, D) 50µm.

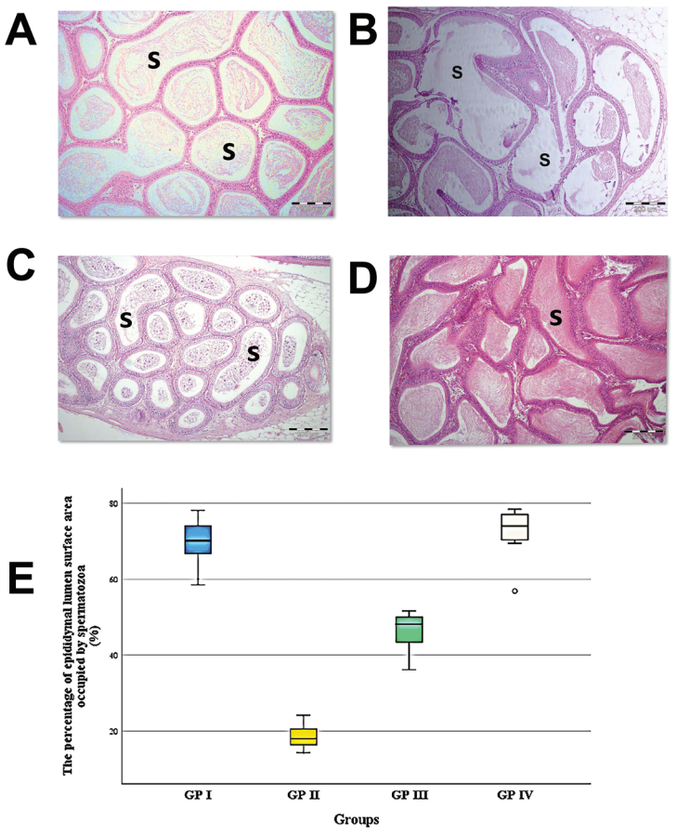

Fig. 7: H&E sections of the epididymis of the different study groups. A; Control group. The epididymis appears lined by pseudostratified columnar epithelium with spermatozoa (s) in the lumen. B; Cis group. The epididymis shows diminished spermatozoa in the lumen. C; Cis+Thq group. The lumen shows spermatozoa along with apparently rounded cells. D; Cis+ThqNLC group. The lumen appears filled with spermatozoa. Microscopic magnification x 100. scale bar: 200µm. E; Comparison between the study groups according to the percentage of epididymal lumen surface area occupied by spermatozoa. Significance detected between (Group II vs {Group I & Group IV}) & (Group III vs {Group I & Group IV})

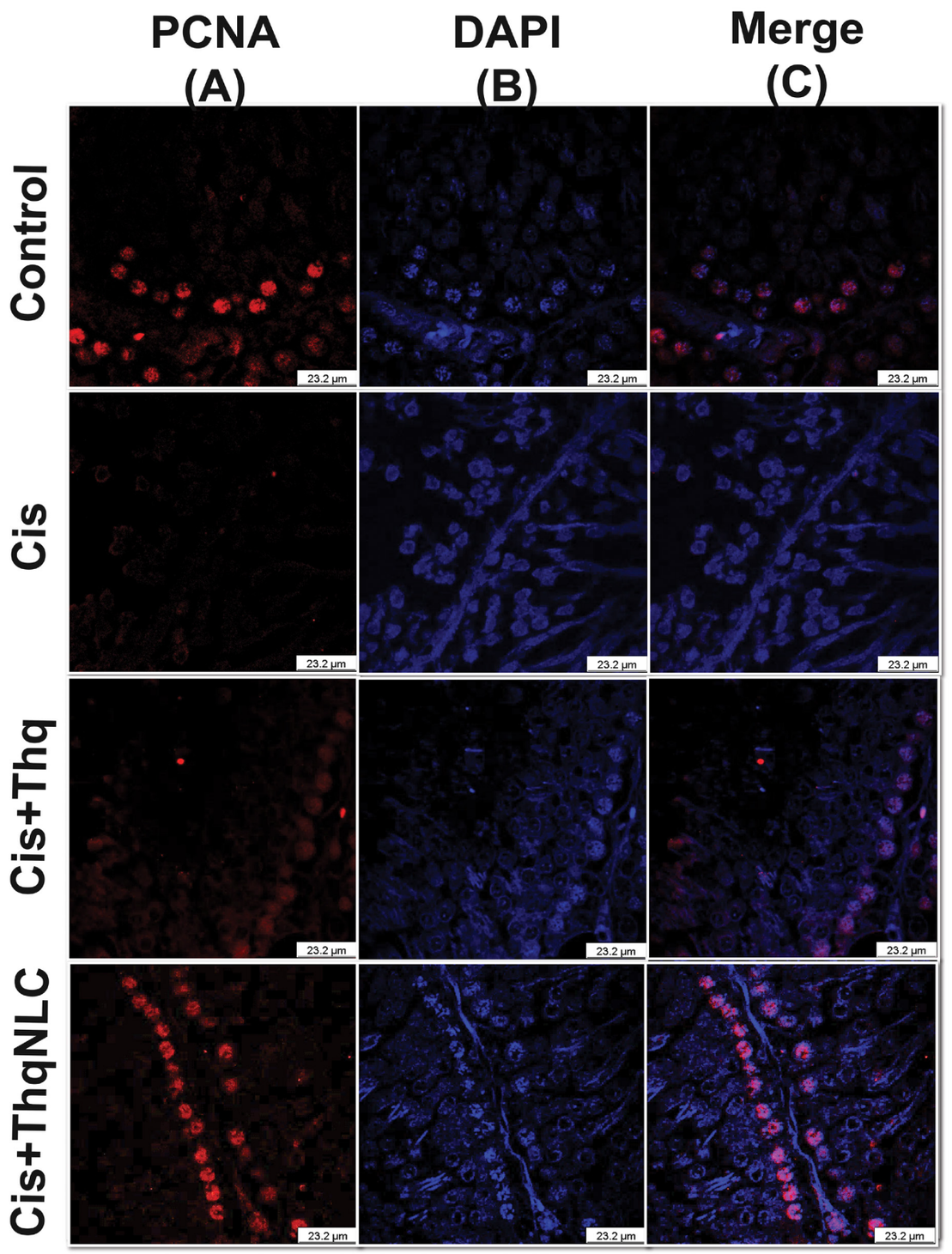

Fig. 8: Confocal laser scanning microscopic photo of rat testis in the study groups. Control; A. The red fluorescence of anti- PCNA immune reaction is evident in spermatogonia resting on the basal lamina with no reaction at the luminal compartment. B. DAPI blue staining shows the nuclei of different cells. C. reveals the nuclear location of anti-PCNA activity. Cis; A. Apparently diminished anti- PCNA immune reaction. B. DAPI blue staining illustrates desquamated spermatogenic cells. Cis+Thq; A. Minimal anti- PCNA immune reaction while DAPI blue staining in (B) illustrates nuclei of partially detached spermatogenic cells from basal lamina. The merged photo (C) reveals the nuclear location of anti-PCNA activity. Cis+ThqNLC; A. Evident anti- PCNA immune reaction in the spermatogonia lying on the basal lamina while DAPI blue staining in (B) illustrates nuclei of spermatogenic cells lining seminiferous tubules. The merged photo (C) reveals the nuclear location of anti-PCNA activity. (CLSM. PCNA immuno-fluorescence (red), DAPI nuclear stain (blue). Mic. Mag. X 630; Scale Bar 23.2µm; Scan Mode =XYZ Unidirectional X, Scan Speed = 400Hz, Pinhole diameter: 136.9µm).

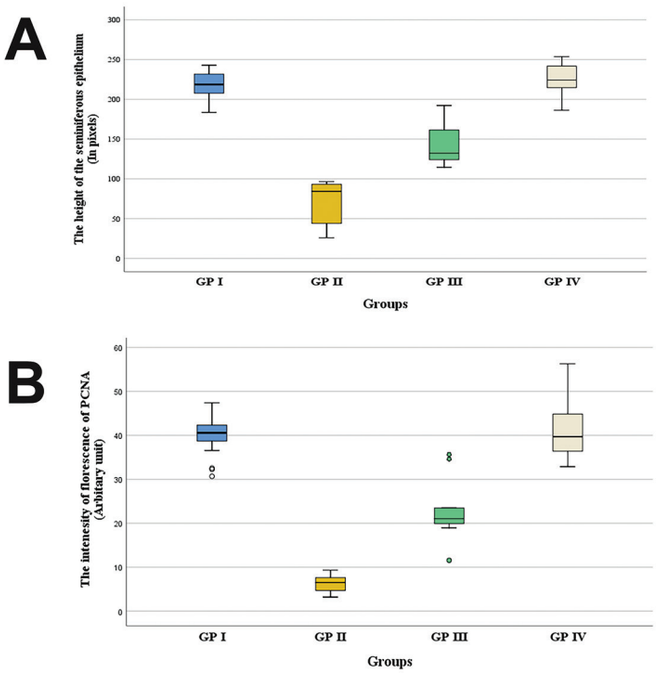

Fig. 9: Comparison between the study groups according to the height of seminiferous epithelium and the intensity of florescence of PCNA. A; The height of the seminiferous epithelium. Significance is detected between (Group II vs {Group I & Group IV}) & (Group III vs {Group I & Group IV}). B; The intensity of florescence of PCNA. Significance is detected between (Group II vs {Group I & Group IV}) & (Group III vs {Group I & Group IV}). Values represent median (min-max), (n = 20). Statistical differences according to Kruskal-Wallis test and Mann-Whitney test for pair wise comparison at ($p< 0.05$).

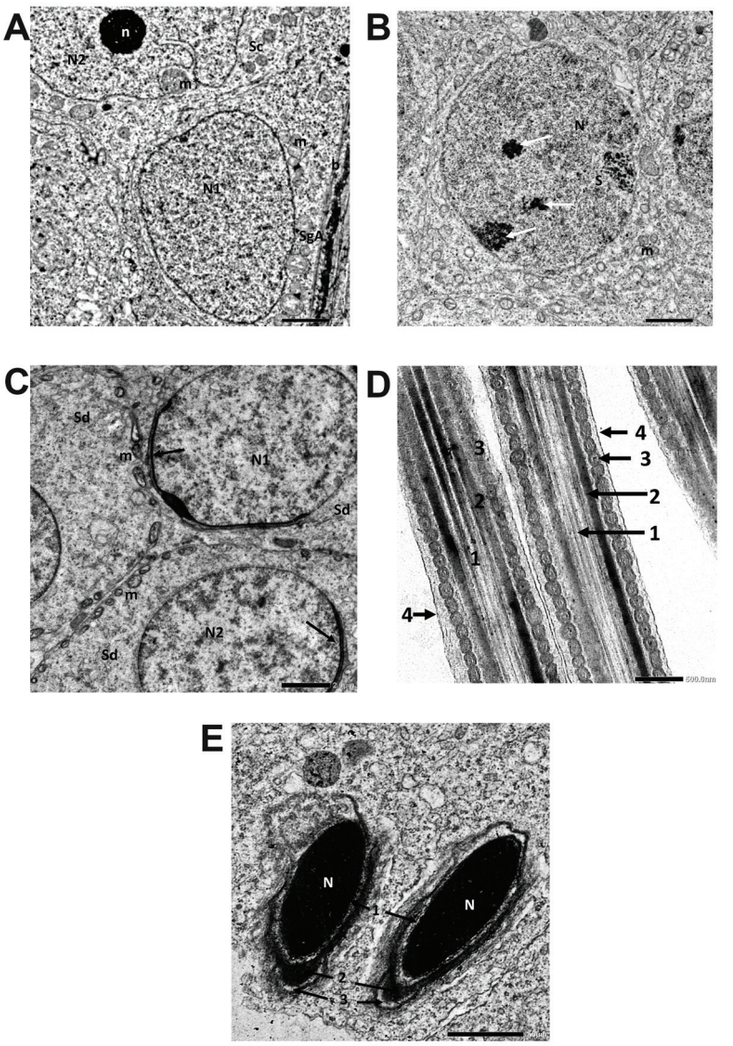

Fig. 10: TEM micrographs of control group. A; Type A spermatogonium (SgA) is seen resting on underlying basal lamina (b). It shows oval euchromatic nucleus (N1) and mitochondria (m). Sertoli cell (Sc) shows indented nucleus (N2) with prominent nucleolus (n) and mitochondria (m*). B; Primary spermatocyte with nucleus (N) showing fine dispersed chromatin granules, areas of condensed chromosomes (arrows) and synaptonemal complex (S). C; Segments of spermatids (Sd) showing well organized mitochondria (m) and euchromatic nuclei with acrosomal cap (arrow). D; Longitudinal section in the middle piece of spermatozoal tail reveals 1. axoneme. 2. outer dense fiber. 3.mitochondrial sheath. 4. flagellar membrane. E; Spermatozoal heads depict an oval dense nucleus (N) surrounded by 1. nuclear envelope 2. acrosomal cap. 3. peri acrosomal space. (Microscopic magnification; A-C X 2500, D X 8000, E X 10000). Scale bar: A-C: 2µm, D: 0.5µm, E: 1µm.

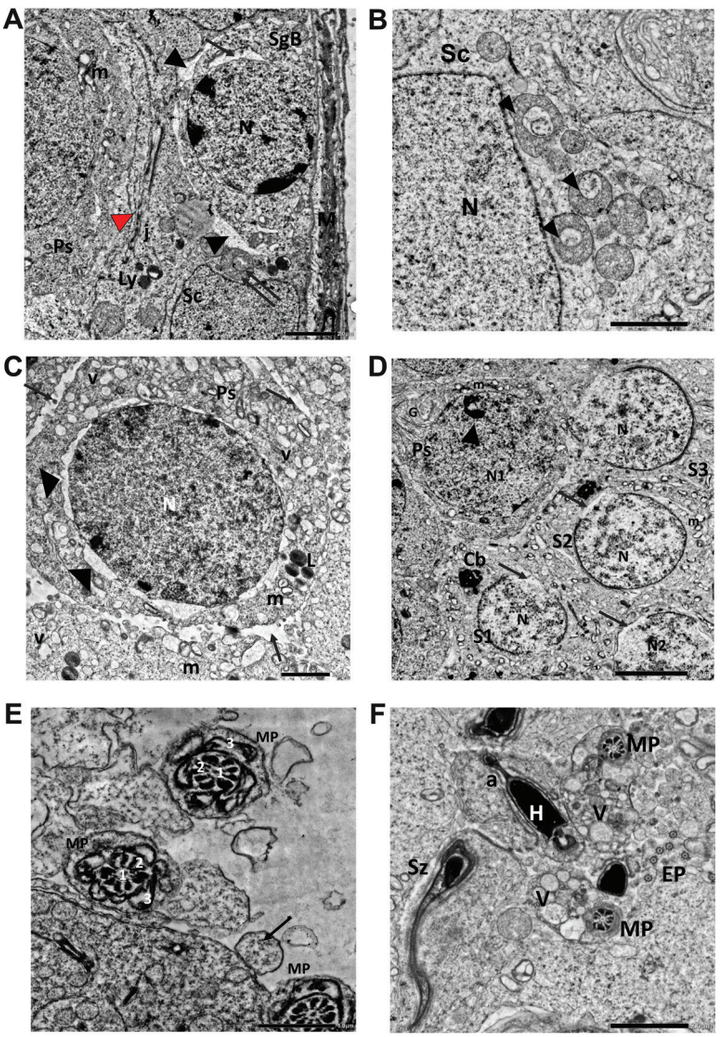

Fig. 11: TEM micrographs of Cis group. A; Type B spermatogonium (SgB) exhibits a rounded nucleus (N) with peripherally located clumps of heterochromatin and dilated perinuclear cisternae (arrow). Arrowheads: wide intercellular spaces. Primary spermatocyte (Ps) shows distorted mitochondria (m). Sertoli cell (Sc) shows lysosomes (Ly) and a mitochondrion with abnormal morphology (annular-shaped mitochondrion) (double arrows) that is located near lysosomes and the nucleus. Red arrowhead: interrupted junctional complex. j: Inter Sertoli junction. B; Part of Sertoli cell (Sc) showing annular appearance of some mitochondria (arrowheads) that are located near the nucleus (N). C; Primary spermatocyte (Ps) with cytoplasmic vacuoles (v), swollen vacuolated mitochondria (m), lysosomes (L), and dilated perinuclear cisterna (arrowhead). Arrows: wide intercellular spaces. D; Primary spermatocyte (Ps) shows a well-developed Golgi complex (G), vacuolated mitochondria (m) & nucleus (N1) with condensed chromatin pattern (arrowhead). Multiple spermatids (S1-S3) with interrupted nuclear envelope (arrows) and vacuolated mitochondria (m). Spermatids' nuclei (N) depict partial chromatin dissolution. N2 shows irregular outline. Cb; Chromatoid body. E; Middle pieces (MP) of spermatozoal tail depict swollen mitochondria with loss of cristae. (1) Axoneme, (2) Outer dense fibers, (3) Mitochondrial sheath. Arrow: residual cytoplasm. F; Abnormal morphology of the spermatozoa (Sz). One of them shows a bizarre shaped acrosomal cap (a) of the head (H). Middle pieces of the tails (MP) show excessive residual vacuolated cytoplasm (V). EP: end piece. (Microscopic magnification; A, B, F X 4000, C X 2500, D X 1500, E X 6000). Scale bar: A-C, F: 2µm, D: 5µm, E: 1µm.

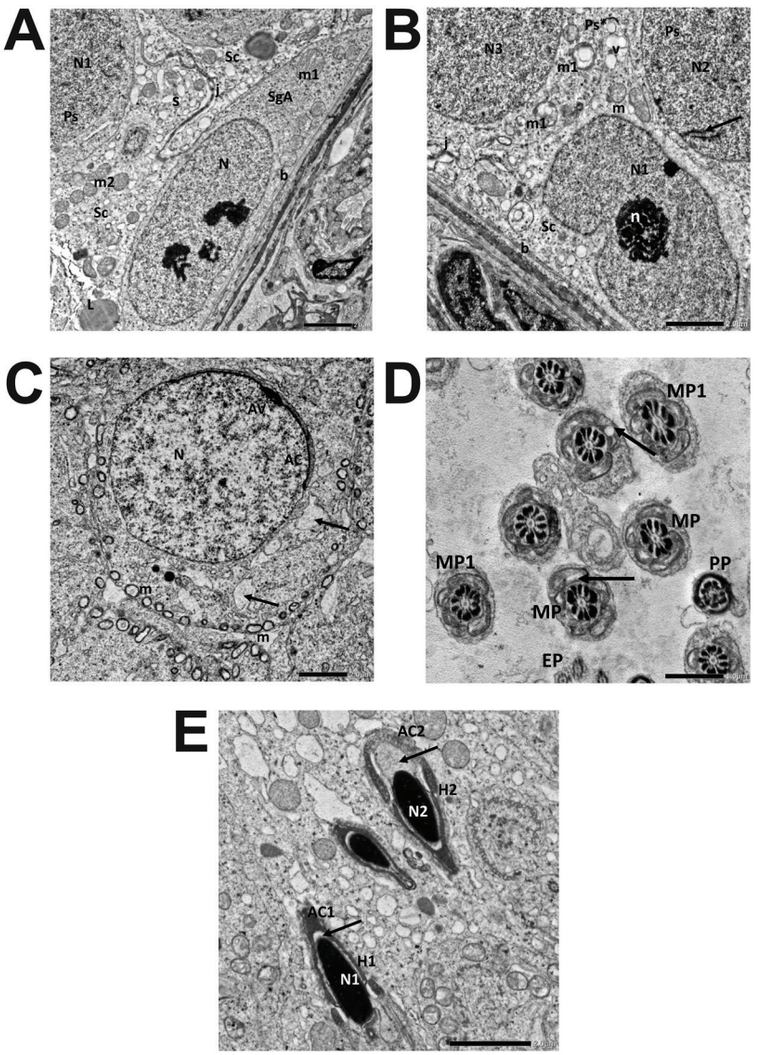

Fig. 12: TEM micrographs of Cis+Thq group. A; Type A spermatogonium (SgA) appears with an oval nucleus (N) that depicts clumps of heterochromatin. A primary spermatocyte (Ps) reveals nucleus (N1) with fine granular chromatin. Parts of Sertoli cells (Sc) are seen. m1: mitochondria of spermatogonium. m2: mitochondria of Sertoli cell. S: smooth endoplasmic reticulum. L: lipid droplets. j: junctional complex. b: basal lamina. B; A Sertoli cell (Sc) with indented nucleus (N1), prominent nucleolus (n) and interrupted intercellular junction (j). It shows cytoplasmic vacuolations (V) and mitochondria (m) with partial loss of cristae. Nuclei (N2 & N3) of two nearby spermatocytes (Ps, Ps*) are noticed, N2 depicts synaptonemal complex (arrow). Vacuolated mitochondria (m1) are noticed in the Ps*. b: the basal lamina. C; Spermatid nucleus (N) is covered by acrosomal vesicle (AV) and acrosomal cap (AC). Focal areas of cytoplasmic rarefaction are noticed (arrows). Deformed mitochondria (m) with disrupted cristae are observed. D; Multiple T.S of spermatozoal tails are seen; middle pieces (MP) depict vacuolated swollen mitochondria (arrows). MP1 appear with almost normal mitochondrial sheath. PP: principal piece. EP: end piece. E; Three spermatozoal heads are seen. H1, H2 depict oval dense nuclei (N1, N2). The acrosomal cap (AC1) appears covering the anterior pole of the nucleus (N1). AC2 appears deformed with excess cytoplasm in sub acrosomal space (arrow) of H2. Microscopic magnification; A, C X 2500, B X 3000, D X 6000, E X 4000). Scale bar: A-C, E: 2µm, D: 1µm.

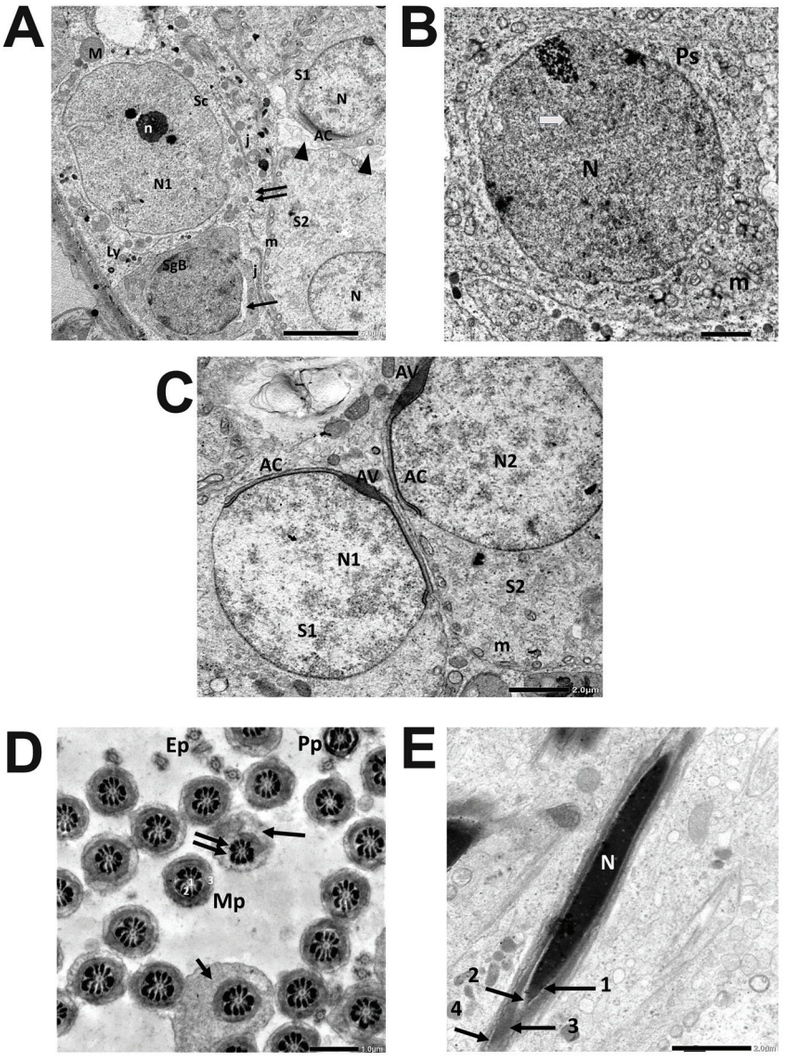

Fig. 13: TEM micrographs of Cis+ThqNLC group. A; Sertoli cell (Sc) with indented nucleus (N1) and tripartite nucleolus (n) is seen. Evident intercellular junction (j) with partial interruption (double arrow). M; mitochondria, Ly; lysosomes. Type B spermatogonium (SgB) shows dilated perinuclear cisterna (arrow). Two spermatids (S1, S2) show partial chromatin dissolution in their nuclei (N) with an acrosomal cap (AC) in S1 and well-organized peripheral mitochondria (m) in S2. Arrow heads: Intercellular spaces. B; Primary spermatocyte (Ps) is seen with nucleus (N) and evident synaptonemal complex (arrow). Some mitochondria (m) with evident cristae are observed. C; A spermatid (S1) depicts a nucleus (N1) with partial karyolysis & S2 reveals a nearly normal nucleus (N2) with acrosomal cap (AC) and acrosomal vesicle (AV).m: mitochondria. D; Transverse sections in spermatozoal tails; Middle pieces (Mp) consist of axoneme (1) at the center surrounded by 9 outer dense fibers (2) and mitochondrial sheath (3). Few middle pieces show excessive residual cytoplasm (arrow) and one shows defects in mitochondrial sheath (double arrow). (Pp): Principal piece (Ep): End pieces. E; Spermatozoal head depicts oval dense nucleus (N) surrounded by: 1. nuclear membrane. 2. sub-acrosomal space. 3. acrosomal cap covering the anterior pole of the nucleus. 4. peri acrosomal space. (Microscopic magnification; A X1500, B X 2500, C X 3000, D X 5000, E X 4000). Scale bar: A: 5µm, B, C, E: 2µm, D: 1µm.

Table 1: Colloidal characteristics and drug loading percentage of ThqNLC

Formulation	Thq conc. (mg)	Particle size (nm)	PDI	Zeta potential (mV)	EE %	Percentage of drug loading
F1	-------	198.2 ± 0.793	0.241 ± 0.021	- 13.7	-------	-------
F2	10	194.3 ± 2.193	0.248 ± 0.011	- 23.4	84.67 ± 1.56	5.92 ± 0.45
F3	20	183.7 ± 0.602	0.217 ± 0.01	- 21.4	91.25 ± 1.23	12.79 ± 1.51
F4	30	195.8 ± 2.159	0.359 ± 0.013	- 21.6	93.80 ± 0.98	15.45 ± 1.23
F5	40	177.5 ± 1.36	0.235 ± 0.015	- 19	96.90 ± 0.67	20.56 ± 0.86
F6	60	196.2 ± 0.4619	0.251 ± 0.006	- 16.3	97.92 ± 1.23	27.56 ± 1.01

DISCUSSION

The burden of deranged fertility in males surviving cases of testicular carcinoma, leukemias and lymphoma, after receiving chemotherapeutic agents especially cisplatin, has drawn attention to be the aim of a huge body of research work[3]. Consequently, several previous studies reported the toxic effects of cisplatin on testis and different possible agents to mitigate this toxicity[4,7,8]. In this context, the current study aimed to investigate the possible protective role of thymoquinone versus thymoquinone loaded on nanostructure lipid carrier, which is regarded as a novel therapeutic approach[9,15,20].

In the present study, the histological and biochemical results of the control subgroups ensured the safety of administration of Thq and its NLC orally in the suggested dose according to the previous studies[24]. Therefore, any changes encountered in the other groups could be associated with cisplatin injections, the testicular toxicity model adopted from previous studies[25].

In cisplatin group, marked histological alteration and tissue distortion were noticed. This deleterious effect can be explained by the excessive production of reactive oxygen species (ROS) with depletion of the tissue antioxidant capacity and impairment of glutathione metabolism leading to a status of oxidative stress, that was confirmed through measuring malondialdehyde (MDA) and total antioxidant capacity (TAC) levels in the rats' sera[7]. Simultaneous increase in lipid peroxidation products with decrease of the overall antioxidant agents' activity were recorded. Measuring TAC was proved to be superior to the analysis of each single antioxidant compound activity alone due to its simplicity and reduced cost and time consumed[38].

It is worth noting that the membranes of the testicular cells are rich in polyunsaturated fatty acids which make them more vulnerable to oxidative stress by ROS. High levels of ROS are very deleterious to the structure of germinal epithelium that normally shows high metabolic activity[39]. Prolonged exposure to high levels of cis-diamminedichloro platinum (II) is the main factor leading to excessive ROS production. Cisplatin acts through depletion of sulfhydryl (SH) group containing compounds like glutathione (GSH), where it is converted to thiyl radicle that subsequently generates ROS from molecular oxygen. This mechanism overweighs the formation of DNA adducts, as the latter accounts only for about 1% of intracellular cisplatin metabolites action[40].

Histological results came in accordance with the biochemical results confirming oxidative stress, where degenerative changes were observed in the spermatogenic cells such as, cytoplasmic vacuolization in the spermatogenic cells, nuclear abnormalities, decreased height of germinal epithelium and desquamated cell debris in the lumen of seminiferous tubules.

The decreased height of germinal epithelium may be partially attributed to apoptosis process[5,41]. Primarily, cisplatin induces apoptosis through activation of p53 leading to cell cycle arrest by inhibiting cyclins and cyclin dependent kinases (CDKs) and stimulation of p21, leading to initiation of the intrinsic pathway of apoptosis[5]. Alteration of the mitochondrial membrane potential, increased permeability in addition to enhanced expression of proapoptotic Bax, Bad and Bak proteins in the outer membrane, lead to release of cytochrome c from the inter-membranous space into the cytoplasm[42]. Subsequently, cytochrome c initiates a cascade of caspases activation. Alteration in the balance between anti-apoptotic Bcl-2 and the pro apoptotic Bax, Bad, and Bak was associated with cisplatin cytotoxicity in an in-vitro study, where it was reported that Cis caused simultaneous decrease in Bcl-2 transcription.[42,43] This is consistent with histological observations, where dark pyknotic nuclei were noticed in spermatogonia and primary spermatocytes with increased intercellular spaces.

Additionally, previous studies reported necrotic changes in association with cisplatin toxicity[41,44,45]. El-Gizawy et al.[46] explained cisplatin induced nephrotoxicity and hepatotoxicity on basis of ROS induced necrosis and inflammation. Cells undergo necrotic changes instead of apoptosis due to higher dose of cisplatin that causes damage to energy related molecules as ATP[41]. Moreover, ROS affect lysosomal integrity that results in release of proteolytic enzymes into the cytosol affecting different organelles including endoplasmic reticulum. Na^+ /H^+ exchanger protein (NHE) is among targets of cisplatin as it leads to increase intra cellular H^+ and increase membrane fluidity through its effect on lipid rafts[6].

Eosinophilic material was observed filling the ST lumens and in the interstitial spaces that also appeared wide. This could be referred to ST's shrinkage and interstitial edema reflecting oxidative stress that induced vascular affection as reported in a previous study of monosodium glutamate induced testicular toxicity. Leakage of the luminal fluid to the interstitium where it was believed to carry germ cell proteins indicating germ cell damage and disruption of blood-testis barrier (BTB)[47,48].

Ultrastructural examination of Sertoli cells revealed abnormal mitochondrial morphology. These findings are suggestive of mitophagy which is considered a subtype of macroautophagy. Mitophagosome was previously described as double membrane bounded damaged mitochondria to be fused with lysosome for elimination. Autophagy is considered a protective mechanism against oxidative and genotoxic stress through engulfing dysfunctional mitochondria[49]. It was noticed that these mitochondria usually exhibit specific distribution around the nucleus and near the lysosomes. This goes with the previously reported result that explained this localization as a step toward autophagosome formation or that mitochondrial membranes shared in the autophagosomes development[50].

Interestingly, a recent study illustrated a unique pathway for mitochondrial self-destruction in neurons

of cases of upper motor neuron lesion. It proposed that the mitochondria are capable of self-destruction independently from lysosomes or autophagosomes in a process named ‘‘mitoautophagy’’. This process was described in successive stages: elongation, curving, fusion of mitochondrial membranes to form annular structure, then finally disintegration[51]. Accordingly, the annular appearance of some mitochondria seen in the cytoplasm of Sertoli cells in Cis group, might represent a stage of mitoautophagy.

Interruptions in inter-Sertoli cells junctions in Cis group was associated with excessive intercellular spaces, and cytoplasmic vacuolation of spermatogenic and Sertoli cells were depicted. These changes were referred to Cis-induced oxidative stress that affected membrane phospholipids leading to impaired cell transport and permeability[52]. In addition, decrease expression of occludin and claudin-2 was recorded in cis toxicity, while minimal effect on ZO-1 was reported, thus explaining disrupted intercellular junctions observed ultra-structurally[53].

Assessing the steroidogenic function of the testis through serum total testosterone level added another explanation to the defective spermatogenesis in Cis group. Another theory was proposed by Saral et al[54] denoting that Cis inhibits testosterone synthesis through 17-α-hydroxylase enzyme suppression or decreasing the numbers of luteinizing hormone (LH) receptors on Leydig cells.

In the present study, defective spermatogenesis was confirmed through histomorphometric analysis of the height of germinal epithelium that revealed statistically significant decrease in Cis group as compared to the control group. In addition, apparent decrease in spermatozoa within the lumina of ST and the cauda epididymis was noticed. Spermatozoa exhibited bizarre shape when seen by electron microscope in the lumina of ST.

Moreover, immunofluorescent analysis results of PCNA came in accordance with the histological results, where markedly diminished immune reaction was encountered in the basal spermatogenic cells thus confirming impaired process of DNA replication and thus the initial steps in process of spermatogenesis.

In the present study, thymoquinone (Thq) loaded on nanostructured lipid carriers (NLC) was used in an attempt to enhance the protective effect of Thq against cisplatin induced testicular toxicity. Lipid based nanocarriers are one of the promising formulations that can increase the solubility of hydrophobic drugs[55]. NLC have several advantages compared to solid lipid nanoparticles and liposomes. NLC have higher drug loading capacity, more stability during storage in addition to their capability to provide better control of drug release[56-58]. This leads to an enhancement in the therapeutic efficacy using safe formulation since previous studies reported the safety of administration of 10 mg/ kg body weight daily[14,59], while the median lethal dose in rats ranged between 794 and 870 mg/kg which is far beyond the administered dose[11].

The study demonstrated the prophylactic effect of thymoquinone as was evident biochemically in groups III and IV where significant decrease in serum level of MDA and increase in TAC were encountered, with more remarkable results in group IV. Histological results came in accordance with the biochemical results, where a relative improvement in the histological alterations of the seminiferous tubules and spermatogenic cells was noticed in Cis+Thq group. However, Cis+ThqNLC group depicted more evident preservation of normal histological features of ST.

Accordingly, the role of the NLC in enhancement of bioavailability of thymoquinone was supported in the current study. This was further confirmed through histomorphometric analysis that demonstrated that the height of germinal epithelium is higher in the Cis+Thq group as compared to Cis group. Notably, the Cis+ThqNLC group demonstrated more significant results as compared to Cis+Thq group where epithelial height is almost in the same range as control. Along with their effect on percentage of epididymal surface area occupied by spermatozoa, where ThqNLC was superior to the ordinary form of Thq.

The results of group III come in accordance with the previous studies, where Thq was used to mitigate doxorubicin and valproic acid induced testicular toxicity[60,61]. Thq exerted its antioxidant mechanism via inhibition of superoxide radicals and lipid peroxidation. In addition, it potentiates the antioxidant enzymes as superoxide dismutase (SOD), catalase, and reduced glutathione (GSH), thus restoring the redox balance[62]. Additionally, it was reported that Thq decreased cyclooxygenase-2 (COX-2) expression, and inflammatory cytokines with subsequent suppression of the inflammatory reaction that is usually associated with oxidative stress. In cases of psoriasis, Thq in a nano-formulation caused diminished levels of interleukins and tumor necrosis factor alpha (TNF-α)[9]. The anti-apoptotic and anti-necrotic effects of Thq were illustrated by Alexander et al[63] in wound healing model where diminished apoptotic figures were documented.

Another postulated beneficial effect of Thq is related to decreased apoptosis of interstitial cells of Leydig and upregulation of aromatase gene expression. Eventually, testosterone secretion is maintained near normal levels[24]. Such an effect was demonstrated in our study, where serum testosterone levels in Cis+Thq and Cis+ThqNLC groups was significantly higher that Cis group.

The protective effect of ThqNLC was referred not only to the original features of thymoquinone, but also to oleic acid -the liquid lipid added in the formulation- which promoted antioxidant capacity, through its previously reported beneficial effects as a naturally occurring fatty acid[24]. This explanation agrees with the previous study of Fahmy et al.[64] who postulated that ThqNLC is more beneficial than the original form of Thq due to its enhanced bioavailability and thus efficacy, and due to other components sharing in their formulation as coconut oil.

CONCLUSION

Eventually, it was concluded that Thq and its NLC form proved their safety on the testicular tissue at the administered dose. In cisplatin toxicity model, ThqNLC was superior to the parent form of the drug in ameliorating testicular affection and restoring spermatogenesis. Nevertheless, further studies are required to assess other possible lipid-based nano-formulation with different Thq doses used.

FUNDING

This research did not receive any specific grant from funding agencies in the public, commercial, or not-for-profit sectors.

CONFLICT OF INTERESTS

There are no conflicts of interest.

REFERENCES

1. Ghosh S. Cisplatin: The first metal based anticancer drug. Bioorg Chem. 2019;88:102925. Doi: 10.1016/j.bioorg.2019.102925.
2. Qi L, Luo Q, Zhang Y, Jia F, Zhao Y, Wang F. Advances in toxicological research of the anticancer drug cisplatin. Chem Res Toxicol. 2019;32(8):1469-1486. Doi: 10.1021/acs.chemrestox.9b00204.
3. Gunnes MW, Lie RT, Bjørge T, Ghaderi S, Ruud E, Syse A, et al. Reproduction and marriage among male survivors of cancer in childhood, adolescence and young adulthood: a national cohort study. Br J Cancer. 2016;114(3):348-356. Doi: 10.1038/bjc.2015.455.
4. Mesbahzadeh B, Hassanzadeh-Taheri M, Aliparast M-s, Baniasadi P, Hosseini M. The protective effect of crocin on cisplatin-induced testicular impairment in rats. BMC Urol. 2021;21(1):1-9. Doi:org/10.1186/s12894-021-00889-2.
5. Tchounwou PB, Dasari S, Noubissi FK, Ray P, Kumar S. Advances in our understanding of the molecular mechanisms of action of cisplatin in cancer therapy. J Exp Pharmacol. 2021;13:303. Doi: 10.2147/JEP.S267383.
6. Makovec T. Cisplatin and beyond: molecular mechanisms of action and drug resistance development in cancer chemotherapy. Radiol Oncol. 2019;53(2):148. Doi: 10.2478/raon-2019-0018.
7. Nna VU, Ujah GA, Suleiman JB, Mohamed M, Nwokocha C, Akpan TJ, et al. Tert-butylhydroquinone preserve testicular steroidogenesis and spermatogenesis in cisplatin-intoxicated rats by targeting oxidative stress, inflammation and apoptosis. Toxicology. 2020;441:152528. Doi: 10.1016/j.tox.2020.152528.
8. Rauf N, Nawaz A, Ullah H, Ullah R, Nabi G, Ullah A, et al. Therapeutic effects of chitosan-embedded vitamin C, E nanoparticles against cisplatin-induced gametogenic and androgenic toxicity in adult male rats. Environ Sci Pollut Res 2021;28(40):56319-56332. Doi: 10.1007/s11356-021-14516-y.
9. El-Far AH, Al Jaouni SK, Li W, Mousa SA. Protective roles of thymoquinone nanoformulations: potential nanonutraceuticals in human diseases. Nutrients. 2018;10(10):1369. Doi: 10.3390/nu10101369.
10. Yimer EM, Tuem KB, Karim A, Ur-Rehman N, Anwar F. Nigella sativa L.(black cumin): a promising natural remedy for wide range of illnesses. Evid Based Complement Alternat Med. 2019;2019:1528635. Doi: org/10.1155/2019/1528635.
11. Ballout F, Habli Z, Rahal ON, Fatfat M, Gali-Muhtasib H. Thymoquinone-based nanotechnology for cancer therapy: promises and challenges. Drug Discov Today. 2018;23(5):1089-1098. Doi: 10.1016/j.drudis.2018.01.043.
12. Mahmoud YK, Abdelrazek HM. Cancer: Thymoquinone antioxidant/pro-oxidant effect as potential anticancer remedy. Biomed Pharmacother. 2019;115:108783. Doi: 10.1016/j.biopha.2019.108783.
13. Zubair H, Khan H, Sohail A, Azim S, Ullah M, Ahmad A, et al. Redox cycling of endogenous copper by thymoquinone leads to ROS-mediated DNA breakage and consequent cell death: putative anticancer mechanism of antioxidants. Cell Death Dis. 2013;4(6):e660. Doi: 10.1038/cddis.2013.172.
14. Ong YS, Saiful Yazan L, Ng WK, Noordin MM, Sapuan S, Foo JB, et al. Acute and subacute toxicity profiles of thymoquinone-loaded nanostructured lipid carrier in BALB/c mice. Int. J. Nanomedicine. 2016;11:5905-5915. Doi: 10.2147/IJN.S114205.
15. Teixeira M, Carbone C, Souto E. Beyond liposomes: Recent advances on lipid based nanostructures for poorly soluble/poorly permeable drug delivery. Prog Lipid Res. 2017;68:1-11. Doi: 10.1016/j.plipres.2017.07.001.
16. Saedi A, Rostamizadeh K, Parsa M, Dalali N, Ahmadi N. Preparation and characterization of nanostructured lipid carriers as drug delivery system: Influence of liquid lipid types on loading and cytotoxicity. Chem Phys Lipids. 2018;216:65-72. Doi: 10.1016/j.chemphyslip.2018.09.007.
17. Zewail M, Nafee N, Helmy MW, Boraie N. Coated nanostructured lipid carriers targeting the joints–an effective and safe approach for the oral management of rheumatoid arthritis. Int J Pharm. 2019;567:118447. Doi: 10.1016/j.ijpharm.2019.118447.
18. Schwarz JC, Baisaeng N, Hoppel M, Löw M, Keck CM, Valenta C. Ultra-small NLC for improved dermal delivery of coenyzme Q10. Int J Pharm. 2013;447(1-2):213-217. Doi: 10.1016/j.ijpharm.2013.02.037.

19. Zewail M, Nafee N, Boraie N. Intra-articular dual drug delivery for synergistic rheumatoid arthritis treatment. J Pharm Sci. 2021;110(7):2808-2822. Doi: 10.1016/j.xphs.2021.04.001.

20. Zafar S, Akhter S, Garg N, Selvapandiyan A, Jain GK, Ahmad FJ. Co-encapsulation of docetaxel and thymoquinone in mPEG-DSPE-vitamin E TPGS-lipid nanocapsules for breast cancer therapy: Formulation optimization and implications on cellular and in vivo toxicity. Eur J Pharm Biopharm. 2020;148:10-26. Doi: 10.1016/j.ejpb.2019.12.016.

21. Daneshmand S, Golmohammadzadeh S, Jaafari MR, Movaffagh J, Rezaee M, Sahebkar A, et al. Encapsulation challenges, the substantial issue in solid lipid nanoparticles characterization. J Cell Biochem. 2018;119(6):4251-4264. Doi: 10.1002/jcb.26617.

22. Ortiz AC, Yañez O, Salas-Huenuleo E, Morales JO. Development of a nanostructured lipid carrier (NLC) by a low-energy method, comparison of release kinetics and molecular dynamics simulation. Pharmaceutics. 2021;13(4):531. Doi: 10.3390/pharmaceutics13040531.

23. Sirikhet J, Chanmahasathien W, Raiwa A, Kiattisin K. Stability enhancement of lycopene in Citrullus lanatus extract via nanostructured lipid carriers. Food Sci Nutr. 2021;9(3):1750-1760. Doi: 10.1002/fsn3.2156.

24. Abdelbaky NW, Abdelazem AZ, Hashem KS. Thymoquinone attenuates 6-mercaptopurine induced testicular toxicity in albino rats: Possible mechanisms are involved. Adv Anim Vet Sci 2020;8(6):653-660. Doi: 10.17582/journal.aavs/2020/8.6.653.660.

25. Zhang K, Weng H, Yang J, Wu C. Protective effect of Liuwei Dihuang Pill on cisplatin-induced reproductive toxicity and genotoxicity in male mice. J Ethnopharmacol. 2020;247:112269. Doi: 10.1016/j.jep.2019.112269.

26. Greenfield EA. Administering anesthesia to mice, rats, and hamsters. Cold Spring Harb Protoc. 2019;2019(6):pdb. prot100198. Doi: 10.1101/pdb.prot100198.

27. Satoh K. Serum lipid peroxide in cerebrovascular disorders determined by a new colorimetric method. Clin Chim Acta. 1978;90(1):37-43. Doi: 10.1016/0009-8981(78)90081-5.

28. Koracevic D, Koracevic G, Djordjevic V, Andrejevic S, Cosic V. Method for the measurement of antioxidant activity in human fluids. J Clin Pathol. 2001;54(5):356-361. Doi: 10.1136/jcp.54.5.356.

29. Fadl AM, Abdelnaby EA, El-Sherbiny HR. Supplemental dietary zinc sulphate and folic acid combination improves testicular volume and haemodynamics, testosterone levels and semen quality in rams under heat stress conditions. Reprod Domest Anim. 2022;57(6):567-576. Doi: 10.1111/rda.14096.

30. Baker HWG. Clinical management of male infertility. In: Jameson JL, De Groot LJ, editors. Endocrinology. 6th ed. Philadelphia: W.B. Saunders; 2010. p. 2556-2579.

31. Bishop ML, Fody EP, Schoeff LE. Clinical Chemistry: Principles, Techniques, and Correlations. 7th ed. Philadelphia: Wolters Kluwer Health; 2013. p. 278-280.

32. Tsuneoka M, Nishimune Y, Ohta K, Teye K, Tanaka H, Soejima M, et al. Expression of Mina53, a product of a Myc target gene in mouse testis. Int J Androl. 2006;29(2):323-330. Doi: 10.1111/j.1365-2605.2005.00572.x.

33. Awaad AK, Kamel MA, Mohamed MM, Helmy MH, Youssef MI, Zaki EI, et al. The role of hepatic transcription factor cAMP response element-binding protein (CREB) during the development of experimental nonalcoholic fatty liver: a biochemical and histomorphometric study. Egypt Liver J. 2020;10(1):1-13. Doi:org/10.1186/s43066-020-00046-8.

34. Suvarna S, Layton C, Bancroft J. Transmission electron microscopy. Bancroft's theory and practice of histological techniques. 8th ed. Oxford: Churchill Livingstone Elsevier; 2019. p. 96-113.

35. Wang TE, Lai YH, Yang KC, Lin SJ, Chen CL, Tsai PS. Counteracting cisplatin-induced testicular damages by natural polyphenol constituent honokiol. Antioxidants. 2020;9(8):723. Doi: 10.3390/antiox9080723.

36. Abdullah F, Nor-Ashikin MNK, Agarwal R, Kamsani YS, Abd Malek M, Bakar NS, et al. Glutathione (GSH) improves sperm quality and testicular morphology in streptozotocin-induced diabetic mice. Asian J Androl. 2021;23(3):281-287. Doi: 10.4103/aja.aja_81_20.

37. Mondal H, Mondal S, Majumder R, De R. Conduct common statistical tests online. Indian Dermatol. Online J.2022;13(4):539-542. Doi: 10.4103/idoj.idoj_605_21.

38. Kusano C, Ferrari B. Total antioxidant capacity: a biomarker in biomedical and nutritional studies. J Cell. Mol Biol. 2008;7(1):1-15.

39. Sahin Z, Ozkaya A, Cuce G, Uckun M, Yologlu E. Investigation of the effect of naringenin on oxidative stress-related alterations in testis of hydrogen peroxide-administered rats. J Biochem Mol Toxicol. 2017;31(9):e21928. Doi: 10.1002/jbt.21928.

40. Dasari S, Tchounwou PB. Cisplatin in cancer therapy: molecular mechanisms of action. Eur J Pharmacol. 2014;740:364-378. Doi: 10.1016/j.ejphar.2014.07.025.

41. Gonzalez VM, Fuertes MA, Alonso C, Perez JM. Is cisplatin-induced cell death always produced by apoptosis? Mol Pharmacol. 2001;59(4):657-663. Doi: 10.1124/mol.59.4.657.

42. Sivalingam KS, Paramasivan P, Weng CF, Viswanadha Vp. Neferine potentiates the antitumor effect of cisplatin in human lung adenocarcinoma cells via a mitochondria-mediated apoptosis pathway. J Cell Biochem. 2017;118(9):2865-2876. Doi: 10.1002/jcb.25937.

43. Chen X, Wei W, Li Y, Huang J, Ci X. Hesperetin relieves cisplatin-induced acute kidney injury by mitigating oxidative stress, inflammation and apoptosis. Chem Biol Interact. 2019;308:269-278. Doi: 10.1016/j.cbi.2019.05.040.

44. Liu Z, Li Z, Chen Z, Li C, Lei L, Wu X, et al. Numb ameliorates necrosis and inflammation in acute kidney injury induced by cisplatin. Chem Biol Interact. 2020;330:109251. Doi: 10.1016/j.cbi.2020.109251.

45. Ekinci-Akdemir FN, Bingöl Ç, Yıldırım S, Kandemir FM, Küçükler S, Sağlam YS. The investigation of the effect of fraxin on hepatotoxicity induced by cisplatin in rats. Iran. J. Basic Med. Sci.2020;23(11):1382. Doi: 10.22038/ijbms.2020.38773.9200

46. El-Gizawy MM, Hosny EN, Mourad HH, Abd-El Razik AN. Curcumin nanoparticles ameliorate hepatotoxicity and nephrotoxicity induced by cisplatin in rats. Naunyn Schmiedebergs Arch. Pharmacol.2020;393:1941-1953. Doi: 10.1007/s00210-020-01888-0.

47. Salama N, Bergh A, Damber J-E. The changes in testicular vascular permeability during progression of the experimental varicocele. Eur Urol. 2003;43(1):84-91. Doi: 10.1016/s0302-2838(02)00501-8.

48. El Kotb SM, El-ghazouly DE-s, Ameen O. The potential cytoprotective effect of Vitamin C and Vitamin E on monosodium glutamate-induced testicular toxicity in rats. Alexandria J. Med.2020;56(1):134-147. Doi: 10.1080/20905068.2020.1804311.

49. Ma X, McKeen T, Zhang J, Ding W-X. Role and mechanisms of mitophagy in liver diseases. Cells. 2020;9(4):837. Doi: 10.3390/cells9040837.

50. Eid N, Ito Y, Horibe A, Otsuki Y, Kondo Y. Ethanol-induced mitochondrial damage in sertoli cells is associated with parkin overexpression and activation of mitophagy. Cells. 2019;8(3):283. Doi: 10.3390/cells8030283.

51. Gautam M, Xie EF, Kocak N, Ozdinler PH. Mitoautophagy: a unique self-destructive path mitochondria of upper motor neurons with TDP-43 pathology take, very early in ALS. Front Cell Neurosci. 2019;13:489. Doi: 10.3389/fncel.2019.00489.

52. ÖZyilmaz Yay N, ŞEner G, Ercan F. Resveratrol treatment reduces apoptosis and morphological alterations in cisplatin induced testis damage. J.Res.Pharm. 2019;23(4):621-631. Doi : 10.12991/jrp.2019.170.

53. Trujillo J, Molina-Jijón E, Medina-Campos ON, Rodríguez-Muñoz R, Reyes JL, Loredo ML, et al. Curcumin prevents cisplatin-induced decrease in the tight and adherens junctions: relation to oxidative stress. Food Funct. 2016;7(1):279-293. Doi: 10.1039/c5fo00624d.

54. Saral S, Ozcelik E, Cetin A, Saral O, Basak N, Aydın M, et al. Protective role of diospyros lotus on cisplatin-induced changes in sperm characteristics, testicular damage and oxidative stress in rats. Andrologia. 2016;48(3):308-317. Doi: 10.1111/and.12448.

55. Hou D, Xie C, Huang K, Zhu C. The production and characteristics of solid lipid nanoparticles (SLNs). Biomaterials. 2003;24(10):1781-1785. Doi: 10.1016/s0142-9612(02)00578-1.

56. Saedi A, Rostamizadeh K, Parsa M, Dalali N, Ahmadi N. Preparation and characterization of nanostructured lipid carriers as drug delivery system: Influence of liquid lipid types on loading and cytotoxicity. Chem Phys Lipids. 2018;216:65-72. Doi: 10.1016/j.chemphyslip.2018.09.007.

57. Ng WK, Saiful Yazan L, Yap LH, Wan Nor Hafiza WAG, How CW, Abdullah R. Thymoquinone-loaded nanostructured lipid carrier exhibited cytotoxicity towards breast cancer cell lines (MDA-MB-231 and MCF-7) and cervical cancer cell lines (HeLa and SiHa). Biomed Res Int. 2015;2015. Doi: 10.1155/2015/263131.

58. Khan S, Baboota S, Ali J, Khan S, Narang RS, Narang JK. Nanostructured lipid carriers: An emerging platform for improving oral bioavailability of lipophilic drugs. Int. J. Pharm. Investig.2015;5(4):182. Doi: 10.4103/2230-973X.167661.

59. Ansar FHZ, Latifah SY, Kamal WHBW, Khong KC, Ng Y, Foong JN, et al. Pharmacokinetics and biodistribution of thymoquinone-loaded nanostructured lipid carrier after oral and intravenous administration into rats. Int. J. Nanomed. 2020;15:7703-7717. Doi: 10.2147/IJN.S262395.

60. Ozturk E, Kaymak E, Akin AT, Karabulut D, Unsal HM, Yakan B. Thymoquinone is a protective agent that reduces the negative effects of doxorubicin in rat testis. Hum Exp Toxicol. 2020;39(10):1364-1373. Doi: 10.1177/0960327120924108.

61. Savran M, Asci H, Armagan I, Erzurumlu Y, Azirak S, Kaya Ozer M, et al. Thymoquinone could be protective against valproic acid-induced testicular toxicity by antioxidant and anti-inflammatory mechanisms. Andrologia. 2020;52(7):e13623. Doi: 10.1111/and.13623.

62. Rathore C, Rathbone MJ, Chellappan DK, Tambuwala MM, Pinto TDJA, Dureja H, et al. Nanocarriers: more than tour de force for thymoquinone. Expert Opin Drug Deliv. 2020;17(4):479-494. Doi: 10.1080/17425247.2020.1730808.

63. Alexander HR, Syed Alwi SS, Yazan LS, Zakarial Ansar FH, Ong YS. Migration and Proliferation Effects of Thymoquinone-Loaded Nanostructured Lipid Carrier (TQ-NLC) and Thymoquinone (TQ) on In Vitro Wound Healing Models. Evid Based Complement Alternat Med. 2019;2019:9725738. Doi: 10.1155/2019/9725738.

64. Fahmy UA, A LA, Awan ZA, Alqarni HM, Alhakamy NA. Optimization of Thymoquinone-Loaded Coconut Oil Nanostructured Lipid Carriers for the Management of Ethanol-Induced Ulcer. AAPS PharmSciTech. 2020;21(5):137. Doi: 10.1208/s12249-020-01693-1.

الملخص العربى

التقييم النسيجي والبيوكيميائي للتأثير الوقائي المحتمل للثيموكينون المحمل على الناقلات الدهنية متناهية الصغر مقابل الثيموكينون على سمية الخصية المحدثة بالسيسبلاتين في الجرذان البالغة

هبة جمال الدين إبراهيم[١]، مشيرة أحمد زهير[١]، فاطمة الزهراء عبد الحميد هاشم[١]، مريم عبد العزيز إبراهيم زويل[٢]، رحاب أحمد عبد المنعم[١]

[١]قسم الهستولوجيا وبيولوجيا الخلية ـ كلية الطب ـ جامعة الإسكندرية.

[٢]قسم الصيدلانيات ـ كلية الصيدلة ـجامعة دمنهور

المقدمة: يعتبر السيسبلاتين حجر الزاوية في أنظمة العلاج الكيميائي المختلفة. ولكن سميته -خاصة على الخصية- تعيق استخدامه. أظهر الثيموكينون قدرات واعدة كمضاد للأكسدة ضد التأثير السلبي للسيسبلاتين. ومع ذلك، نظرًا لانخفاض التوافر البيولوجي بعد تناوله عن طريق الفم، فقد تم تطوير الناقلات الدهنية متناهية الصغر المحملة بالثيموكينون.

الهدف: لمقارنة التأثير الوقائي المحتمل للثيموكينون المحمل على الناقلات الدهنية متناهية الصغر مقابل الثيموكينون للتخفيف من التأثيرات المرضية المحدثة بالسيسبلاتين على الخصية.

المواد وطرق البحث: تم تقسيم ذكور الجرذان البيضاء إلى أربعة مجموعات، كل مجموعة من أثني عشر جرذا في تجربة مدتها شهراً واحداً: المجموعة الأولى: هي المجموعة الضابطة (قسمت الي ثلاثة مجموعات: ا وب وج) و تناولت عن طريق الفم: ماءً مقطر اً و الثيموكينون (٥ مجم / كجم يوميًا) و الثيموكينون المحمل علي الناقلات الدهنية متناهية الصغر (٥ مجم / كجم يوميًا) علي التوالي، المجموعة الثانية تم حقنها بالسيسبلاتين في الغشاء البيتوني مرة واحدة يوميًا من اليوم ١١ إلى اليوم ١٥ (٣مجم / كجم). المجموعة الثالثة تم حقنها بالسيسبلاتين في الغشاء البيتوني مع تناول الثيموكينون عن طريق الفم. المجموعة الرابعة: تم حقنها بالسيسبلاتين في الغشاء البيتوني مع تناول الثيموكينون المحمل علي الناقلات الدهنية متناهية الصغر عن طريق الفم. تم تقييم التأثير على الخصية من خلال الدراسات النسيجية والمورفومترية. تم تقييم المؤشرات المصلية مثل المالون دايالداهيد والقدرة الكلية لمضادات الأكسدة وإجمالي هرمون التستوستيرون في الدم. بالإضافة إلى ذلك، تم دراسة تفاعل التألق المناعي ضد مستضد تكاثر الخلية النووي بواسطة المجهر الماسح بالليزر المتحد البؤر.

النتائج: أثبتت الدراسة أمان استخدام الثيموكينون المحمل على الناقلات الدهنية متناهية الصغر في الجرعة المعطاة بالإضافة إلى دوره في تخفيف سمية الخصية الذي تفوق على الثيموكينون في حالته العادية. ظهرت هذه القدرة الوقائية واضحة من خلال النتائج النسيجية والبيوكيميائية التي أشارت إلى قدرة الثيموكينون المحمل على الناقلات الدهنية متناهية الصغر كمضاد للأكسدة كما يتضح من الاختلافات الملحوظة في مستويات المالون دايالداهيد والقدرة الكلية لمضادات الأكسدة بين مجموعات الدراسة.

الاستنتاج: أظهر الثيموكينون المحمل على الناقلات الدهنية متناهية الصغر تأثيرًا وقائيًا ضد سمية الخصية المحدثة بالسيسبلاتين، وبالتالي، يمكن للثيموكينون أن يلعب دورًا أساسيًا في مجال الخصوبة والأورام.